A central discontinuous Galerkin method for Hamilton-Jacobi equations

Fengyan Li [1] and Sergey Yakovlev [2]

Abstract

In this paper, a central discontinuous Galerkin method is proposed to solve for the viscosity solutions of Hamilton-Jacobi equations. Central discontinuous Galerkin methods were originally introduced for hyperbolic conservation laws. They combine the central scheme and the discontinuous Galerkin method and therefore carry many features of both methods. Since Hamilton-Jacobi equations in general are not in the divergence form, it is not straightforward to design a discontinuous Galerkin method to directly solve such equations. By recognizing and following a "weighted-residual" or "stabilization-based" formulation of central discontinuous Galerkin methods when applied to hyperbolic conservation laws, we design a high order numerical method for Hamilton-Jacobi equations. The L^2 stability and the error estimate are established for the proposed method when the Hamiltonians are linear. The overall performance of the method in approximating the viscosity solutions of general Hamilton-Jacobi equations are demonstrated through extensive numerical experiments, which involve linear, nonlinear, smooth, nonsmooth, convex, or nonconvex Hamiltonians.

Keywords: discontinuous Galerkin method, central scheme, Hamilton-Jacobi equation, viscosity solution, high order accuracy

AMS subject classification: 65M60, 65M12, 35L60

[1]Department of Mathematical Sciences, Rensselaer Polytechnic Institute, Troy, NY, 12180. E-mail: lif@rpi.edu. The research was supported in part by the NSF under the grant DMS-0652481, NSF CAREER award DMS-0847241 and by an Alfred P. Sloan Research Fellowship. Additional support was provided by NSFC grant 10671091 while Li was visiting Department of Mathematics at Nanjing University, China.

[2]Department of Mathematical Sciences, Rensselaer Polytechnic Institute, Troy, NY, 12180. E-mail: yakovs@rpi.edu. The research was supported in part by the NSF CAREER award DMS-0847241.

1 Introduction

Hamilton-Jacobi (H-J) equation

$$\partial_t \varphi(\mathbf{x}, t) + H(\mathbf{x}, \varphi(\mathbf{x}, t), \nabla_{\mathbf{x}} \varphi(\mathbf{x}, t)) = 0, \ \mathbf{x} \in \Omega \subset \mathbb{R}^d \tag{1.1}$$

with suitable initial and boundary conditions arises in various applications, such as optimal control, differential games, seismic waves, crystal growth, robotic navigation, image processing and calculus of variations. The solution of such equation may develop discontinuous derivatives in finite time even when the initial data is smooth, indicating the classical solutions may not always exist. To ensure the existence of the solution as well as to single out the physically relevant solution, the concept of viscosity solutions was established for H-J equations. Such development is due to Crandall, Evans and Lions among many others, see e.g. [16, 15]. Throughout the paper, the Hamiltonian $H(\mathbf{x}, q, \mathbf{p})$ in (1.1) is called linear (resp. nonlinear, smooth, nonsmooth, convex, nonconvex) when it is linear (resp. nonlinear, smooth, nonsmooth, convex, nonconvex) with respect to $\mathbf{p}$.

Since the early work by Crandall and Lions [17] and Souganidis [38], there have been many numerical methods developed to solve for the viscosity solution of (1.1). Because of the focus of this paper, some of these methods with high order accuracy are listed here, such as essentially nonoscillatory (ENO) schemes [33, 34], weighted ENO (WENO) and Hermite WENO schemes [21, 40, 35], central schemes [24, 22, 5], and discontinuous Galerkin methods [20, 27, 6]. The primary goal of this paper is to design a high order numerical method, namely, a central discontinuous Galerkin (DG) method, to solve H-J equations for their viscosity solutions.

DG finite element methods were originally devised for conservation laws [36, 12, 11, 10, 7, 13] and later for many other applications, see, e.g. [8, 1, 14]. Compared with other methods, DG methods have many attractive features such as being flexible with complicated geometries, different boundary conditions, and various local approximations [9, 27, 39], using compact stencils to achieve high order accuracy, and the easy parallel implementation. Till

now there are mainly two DG methods available for solving H-J equations. Both were formulated when the Hamiltonian H in (1.1) is in the form of $H(\mathbf{x}, \nabla_{\mathbf{x}}\varphi(\mathbf{x}, t))$, that is,

$$\partial_t \varphi(\mathbf{x}, t) + H(\mathbf{x}, \nabla_{\mathbf{x}}\varphi(\mathbf{x}, t)) = 0, \ \mathbf{x} \in \Omega \subset \mathbb{R}^d \tag{1.2}$$

And they can be extended to the general H-J equation (1.1). The first approach is based on the elegant connection between the H-J equation and the conservation law system. Notice by differentiating (1.2) with respect to $\mathbf{x}$, one obtains a conservation system for the gradient field $\mathbf{w} = \nabla_{\mathbf{x}}\varphi$,

$$\partial_t \mathbf{w}(\mathbf{x}, t) + \nabla_{\mathbf{x}} H(\mathbf{x}, \mathbf{w}(\mathbf{x}, t)) = \mathbf{0}, \ \mathbf{x} \in \Omega \subset \mathbb{R}^d. \tag{1.3}$$

Different from the standard conservation system, the components of $\mathbf{w}$ are not independent. By following the derivation of DG methods for conservation laws, in addition with a least squares procedure in each time step (or each time stage depending on the particular time discretization used) if (1.3) is multi-dimensional, a DG method was proposed in [20]. The method first solves for $\mathbf{w}$, then the missing constant in φ is recovered based on the original equation (1.2). Later this method was reinterpreted and simplified by Li and Shu in [27], with the use of locally curl-free approximations for $\mathbf{w}$ in a standard DG framework. This is based on the intrinsic structure of $\mathbf{w}$: $\mathrm{curl}_{\mathbf{x}}\mathbf{w} = \mathrm{curl}_{\mathbf{x}}\nabla_{\mathbf{x}}\varphi = 0$. The new equivalent formulation in [27] avoids the use of the least squares procedure and involves fewer unknowns, and therefore reduces the overall computational complexity for multi-dimensional cases. Moreover, it recasts the DG method for H-J equations in [20, 25] into the method of lines framework, which is more natural for analysis and implementation.

The DG method reviewed above reliably captures the viscosity solutions of (1.2). In terms of accuracy, it is optimal for $\nabla_{\mathbf{x}}\varphi$ and in general suboptimal for φ itself with respect to the approximation properties of discrete spaces. On the other hand, the method is based on differential equations for $\nabla_{\mathbf{x}}\varphi$, and in multi-dimensional cases, a single equation (1.2) is converted to a system of equations (1.3). In addition, the solutions of (1.2) are often smoother than those of (1.3). This motivates the development of the second DG method in

[6] to *directly* solve (1.2). However it is not straightforward to design a direct method for H-J equations in the DG framework. With one dimension as an example, notice the equation (1.2) contains $H(x, \partial_x \varphi)$ and it is in general not in the divergence form. When (1.2) is multiplied by a test function and integrated, using integration by parts can not further shift the differential operator in space from φ to the test function, a simple but commonly used step to define weak solutions and to design DG methods for many applications.

On the other hand, the "weighted-residual" or "stabilization-based" formulations of DG methods for linear PDEs are discussed in [3, 2], which reveal in many DG methods the balance of "how the numerical solution satisfies the PDE locally", "how the continuity of certain qualities is imposed across element interfaces" and even "how the boundary condition is satisfied". The method proposed in [6] can be regarded as a DG method with such structure yet for equations which might be nonlinear. For linear Hamiltonians with discontinuous coefficients or for nonlinear Hamiltonians, since the "weighted-residual" type method alone in [6] is of Roe type, the scheme may generate entropy violating solutions. To ensure the convergence to viscosity solutions, an additional entropy correction procedure was adopted. The L^2 stability and the optimal error estimate are established when the Hamiltonian is linear with smooth coefficients. For nonlinear cases with convex Hamiltonians, numerical experiments demonstrate the stability and the optimal accuracy of the overall scheme.

In this paper, we propose a high order numerical method, namely, a central DG method, to *directly* solve for the viscosity solutions of H-J equations. Central DG methods were introduced in [28, 30, 31] for hyperbolic conservation laws, and they combine the central scheme [32, 23, 29] and the DG method. These methods evolve two copies of approximating solutions defined on overlapping meshes, and they avoid the use of Riemann solvers which can be complicated and costly for system of equations [26]. The co-existence of two numerical solutions also provides new opportunities, and one such example is the nonoscillatory hierarchical reconstruction based on both solutions discussed in [30]. Besides, the methods carry many features of standard DG methods.

What motivates the scheme in this paper is the observation that the central DG method, when solving hyperbolic conservation laws [30], can be rewritten into a "weighted-residual" or "stabilization-based" formulation [3, 2]. By following the structure of such formulation, and with the similar treatment as in [6] to impose the continuity of the solution across element interfaces, we introduce a central DG method for H-J equations (1.1). When $H(\mathbf{x}, \varphi, \nabla_{\mathbf{x}}\varphi) = \mathbf{c}\cdot\nabla_{\mathbf{x}}\varphi$ with $\mathbf{c}$ being a constant field, the H-J equation is also a conservation equation, and the proposed method is the same as the one in [30]. When the method is applied to H-J equations with linear Hamiltonians, we establish the L^2 stability and the error estimate. This estimate is suboptimal with respect to the approximation properties of discrete spaces, however, we always observe the optimal accuracy of the proposed method for smooth solutions. In addition, a nonlinear limiting strategy is introduced in order to capture the viscosity solutions for some examples with nonconvex Hamiltonians, see Section 2.2 and Section 4. The overall performance of the proposed method in terms of high order accuracy and reliability, when approximating the viscosity solutions of general H-J equations, is demonstrated through a series of numerical experiments which involve linear, nonlinear, smooth, nonsmooth, convex, or nonconvex Hamiltonians.

The rest of this paper is organized as follows. In Section 2, a central DG method is motivated and formulated for H-J equations. Theoretical analysis in terms of the L^2 stability and the error estimate for linear Hamiltonian cases is carried out in Section 3. In Section 4, a collection of one and two dimensional numerical examples are presented to demonstrate the performance of the proposed method, which are followed by concluding remarks in Section 5.

2 Numerical scheme

To motivate the scheme, we start with a brief review of the central DG method when applied to a one dimensional scalar conservation equation

$$\partial_t \varphi(x,t) + \partial_x f(\varphi(x,t)) = 0, \qquad x \in (0,a). \tag{2.1}$$

For simplicity, the periodic boundary condition is assumed. The method can also be defined for multi-dimensional or system cases with general boundary conditions. Let $\{x_i\}_i$ be a partition of $[0,a]$ with $x_{i+\frac{1}{2}}=\frac{1}{2}(x_i+x_{i+1})$, $I_i=(x_{i-\frac{1}{2}},x_{i+\frac{1}{2}})$ and $I_{i+\frac{1}{2}}=(x_i,x_{i+1})$. Two discrete spaces associated with overlapping meshes $\{x_i\}_i$ and $\{x_{i+\frac{1}{2}}\}_i$ are defined

$$V_h=V_h^k=\{v:v\big|_{I_i}\in P^k(I_i),\forall i\},\qquad W_h=W_h^k=\{v:v\big|_{I_{i+\frac{1}{2}}}\in P^k(I_{i+\frac{1}{2}}),\forall i\}$$

where $P^k(I)$ is the set of polynomials with the degree at most k on I. We further denote $w(x^{\pm})=\lim_{\epsilon\to 0\pm}w(x+\epsilon)$, and the jump of w at x_i, $x_{i+\frac{1}{2}}$ as $[w]_i=w(x_i^+)-w(x_i^-)$, $[w]_{i+\frac{1}{2}}=w(x_{i+\frac{1}{2}}^+)-w(x_{i+\frac{1}{2}}^-)$ respectively.

To solve (2.1), the central DG method uses both spaces V_h and W_h and its semi-discrete formulation is given as follows [30]: find $\varphi_h(\cdot,t)\in V_h$ and $\psi_h(\cdot,t)\in W_h$, such that for any $\eta\in V_h$, $\xi\in W_h$ and for all i,

$$\begin{aligned}\int_{I_i}\partial_t\varphi_h\eta dx=&\frac{1}{\tau_{\max}}\int_{I_i}(\psi_h-\varphi_h)\eta dx+\int_{I_i}f(\psi_h)\eta_x dx\\&-f\left(\psi_h(x_{i+\frac{1}{2}},t)\right)\eta(x_{i+\frac{1}{2}}^-)+f\left(\psi_h(x_{i-\frac{1}{2}},t)\right)\eta(x_{i-\frac{1}{2}}^+),\end{aligned}\tag{2.2}$$

$$\begin{aligned}\int_{I_{i+\frac{1}{2}}}\partial_t\psi_h\xi dx=&\frac{1}{\tau_{\max}}\int_{I_{i+\frac{1}{2}}}(\varphi_h-\psi_h)\xi dx+\int_{I_{i+\frac{1}{2}}}f(\varphi_h)\xi_x dx\\&-f\left(\varphi_h(x_{i+1},t)\right)\xi(x_{i+1}^-)+f\left(\varphi_h(x_i,t)\right)\xi(x_i^+).\end{aligned}\tag{2.3}$$

Here $\tau_{\max}$ is the maximal time step allowed by the stability condition. It is more suitable to write $\tau_{\max}=\tau_{\max}(t)$, as in implementation $\tau_{\max}$ is often dynamically chosen and it is closely related to the actual time step, see Section 4. One can refer to [29, 30] for the origin of $\tau_{\max}$. The key observation that motivates the proposed scheme is the following reformulation of (2.2)-(2.3), after integration by parts with respect to x,

$$\int_{I_i}\left(\partial_t\varphi_h+\partial_x f(\psi_h)\right)\eta dx=\frac{1}{\tau_{\max}}\int_{I_i}(\psi_h-\varphi_h)\eta dx-[f(\psi_h)]_i\eta(x_i),\tag{2.4}$$

$$\int_{I_{i+\frac{1}{2}}}\left(\partial_t\psi_h+\partial_x f(\varphi_h)\right)\xi dx=\frac{1}{\tau_{\max}}\int_{I_{i+\frac{1}{2}}}(\varphi_h-\psi_h)\xi dx-[f(\varphi_h)]_{i+\frac{1}{2}}\xi(x_{i+\frac{1}{2}}).\tag{2.5}$$

Notice that the first term in each of the above equations is a "generalized residual" in the sense that if $\varphi_h=\psi_h$, this term measures how φ_h satisfies the PDE (2.1) locally. (2.4)

and (2.5) reflect a balance between such generalized residual, continuity of the flux function $f(\cdot)$ at the element interfaces, and the difference of two approximating solutions φ_h and ψ_h. DG methods with similar structures defined on one mesh, termed as DG methods in the "weighted-residual" or "stabilization-based" formulations, are discussed in [3, 2] for linear PDEs.

Based on the central DG method for hyperbolic conservation laws with the structure of (2.4)-(2.5) as well as the direct DG method for solving H-J equations introduced by Cheng and Shu [6], with the same notations as introduced above for meshes and discrete spaces V_h and W_h, we propose the following central DG method for the one dimensional H-J equation (1.1): look for $\varphi_h(\cdot,t) \in V_h$ and $\psi_h(\cdot,t) \in W_h$, such that for any $\eta \in V_h$, $\xi \in W_h$ and for all i,

$$\int_{I_i} (\partial_t \varphi_h + H(x, \psi_h, \partial_x \psi_h))\, \eta dx = \frac{1}{\tau_{\max}} \int_{I_i} (\psi_h - \varphi_h)\eta dx - H_1(x, \varphi_h, \partial_x \varphi_h)|_{x=x_i} [\psi_h]_i \eta(x_i), \tag{2.6}$$

$$\int_{I_{i+\frac{1}{2}}} (\partial_t \psi_h + H(x, \varphi_h, \partial_x \varphi_h))\, \xi dx = \frac{1}{\tau_{\max}} \int_{I_{i+\frac{1}{2}}} (\varphi_h - \psi_h)\xi dx - H_1(x, \psi_h, \partial_x \psi_h)|_{x=x_{i+\frac{1}{2}}} [\varphi_h]_{i+\frac{1}{2}} \xi(x_{i+\frac{1}{2}}), \tag{2.7}$$

where $H_1(x,q,p) = \frac{\partial}{\partial p} H(x,q,p)$, the characteristic speed of (1.1) according to its characteristic equations [18]. Though the treatment for the jumps of φ_h and ψ_h at element interfaces is similar to the one in [6], the terms involving $\varphi_h - \psi_h$ introduce additional stabilization mechanism and therefore the proposed scheme is reliable to capture the viscosity solutions without any additional entropy correction procedure, see Theorem 3.1 in Section 3 and numerical examples in Section 4.

The method proposed above can also be defined for multi-dimensional H-J equations with structured or unstructured meshes. For simplicity, we here consider a two dimensional domain $\Omega = [0,a] \times [0,b]$ with overlapping rectangular meshes. Let $\{x_i\}_i$ and $\{y_j\}_j$ be partitions of $[0,a]$ and $[0,b]$ respectively, with $x_{i+\frac{1}{2}} = \frac{1}{2}(x_i + x_{i+1})$, $I_i = (x_{i-\frac{1}{2}}, x_{i+\frac{1}{2}})$, $I_{i+\frac{1}{2}} = (x_i, x_{i+1})$, and $y_{j+\frac{1}{2}} = \frac{1}{2}(y_j + y_{j+1})$, $J_j = (y_{j-\frac{1}{2}}, y_{j+\frac{1}{2}})$, $J_{j+\frac{1}{2}} = (y_j, y_{j+1})$. Then $\{D_{i,j}\}_{i,j}$ and $\{D_{i+\frac{1}{2},j+\frac{1}{2}}\}_{i,j}$ define two overlapping meshes for Ω, with $D_{i,j} = I_i \times J_j$ and $D_{i+\frac{1}{2},j+\frac{1}{2}} =$

$I_{i+\frac{1}{2}} \times J_{j+\frac{1}{2}}$, see Figure 2.1. Associated with these meshes, one can define two discrete spaces:

$$V_h = V_h^k = \{v : v\big|_{D_{i,j}} \in P^k(D_{i,j}), \forall i, j\}, \quad W_h = W_h^k = \{v : v\big|_{D_{i+\frac{1}{2},j+\frac{1}{2}}} \in P^k(D_{i+\frac{1}{2},j+\frac{1}{2}}), \forall i, j\}.$$

Here $P^k(D)$ is the set of polynomials with the *total* degree at most k on D.

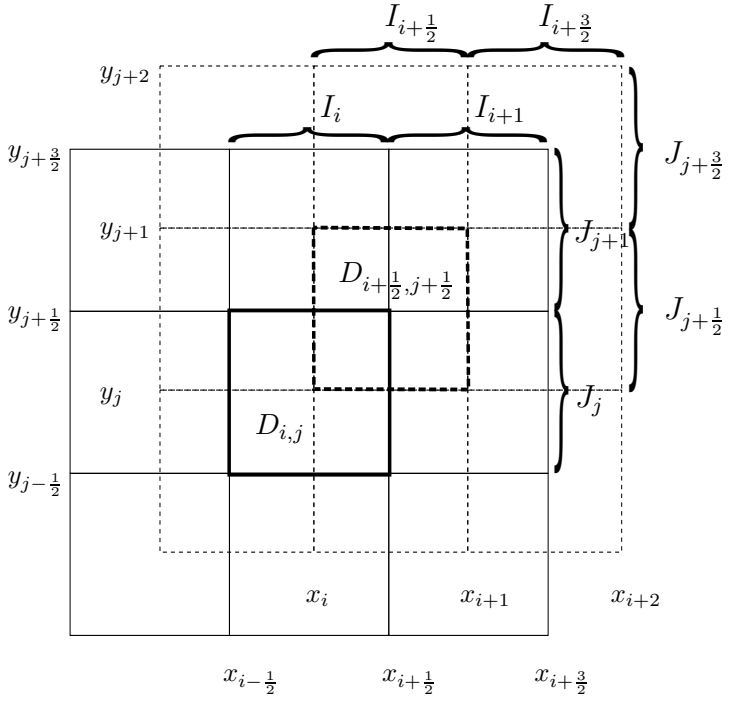

Figure 2.1: Two dimensional overlapping meshes

Similar to one dimensional cases, a central DG method for two dimensional H-J equations (1.1) is defined as follows: look for $\varphi_h(.,t) \in V_h$ and $\psi_h(.,t) \in W_h$, such that for any $\eta \in V_h$, $\xi \in W_h$ and for all i and j,

$$\begin{aligned}\int_{D_{i,j}} (\partial_t \varphi_h + H(\mathbf{x}, \psi_h, \nabla_{\mathbf{x}} \psi_h))\, \eta d\mathbf{x} = &\frac{1}{\tau_{\max}} \int_{D_{i,j}} (\psi_h - \varphi_h)\eta d\mathbf{x} \\ &- \int_{J_j} H_1(\mathbf{x}, \varphi_h, \nabla_{\mathbf{x}}\varphi_h)\big|_{x=x_i} [\psi_h(\cdot, y)]_i \eta(x_i, y) dy \\ &- \int_{I_i} H_2(\mathbf{x}, \varphi_h, \nabla_{\mathbf{x}}\varphi_h)\big|_{y=y_j} [\psi_h(x, \cdot)]_j \eta(x, y_j) dx,\end{aligned}$$

$$\int_{D_{i+\frac{1}{2},j+\frac{1}{2}}} \left(\partial_t \psi_h + H(\mathbf{x}, \varphi_h, \nabla_{\mathbf{x}}\varphi_h)\right) \xi d\mathbf{x} = \frac{1}{\tau_{\max}} \int_{D_{i+\frac{1}{2},j+\frac{1}{2}}} (\varphi_h - \psi_h)\xi d\mathbf{x}$$
$$- \int_{J_{j+\frac{1}{2}}} H_1(\mathbf{x}, \psi_h, \nabla_{\mathbf{x}}\psi_h)\big|_{x=x_{i+\frac{1}{2}}} [\varphi_h(\cdot, y)]_{i+\frac{1}{2}} \xi(x_{i+\frac{1}{2}}, y) dy$$
$$- \int_{I_{i+\frac{1}{2}}} H_2(\mathbf{x}, \psi_h, \nabla_{\mathbf{x}}\psi_h)\big|_{y=y_{j+\frac{1}{2}}} [\varphi_h(x, \cdot)]_{j+\frac{1}{2}} \xi(x, y_{j+\frac{1}{2}}) dx.$$

Here $\big(H_1(x, q, \mathbf{p}), H_2(x, q, \mathbf{p})\big) = \nabla_{\mathbf{p}} H(x, q, \mathbf{p})$, which is related to the characteristic speed of H-J equations [18], and $\tau_{\max}$ is the maximal time step allowed by the stability condition [29, 30].

Remark 2.1. When $H(\mathbf{x}, \varphi, \nabla_{\mathbf{x}}\varphi) = \mathbf{c} \cdot \nabla_{\mathbf{x}}\varphi$ with $\mathbf{c}$ being a constant field, the H-J equation is also a conservation equation, and the proposed method is the same as the one in [30]. When (1.1) is nonlinear, the proposed scheme is consistent only when $k \geq 1$. Take one dimensional Burgers' equation as an example, that is, $H(x, \varphi, \partial_x\varphi) = \frac{1}{2}(\partial_x\varphi)^2$ and $H_1(x, \varphi, \partial_x\varphi) = \partial_x\varphi$. When $k = 0$, $\partial_x\varphi_h\big|_{I_i} = \partial_x\psi_h\big|_{I_{i+\frac{1}{2}}} = 0, \forall\, i$, all terms containing $H(x, q, p)$ and $H_1(x, q, p)$ in (2.6)-(2.7) vanish, and this implies that the scheme is inconsistent to the Burgers' equation. Such inconsistency can be avoided by reconstructing the numerical derivative for a piecewise constant function, and such remedy is not pursued in this paper.

2.1 Numerical boundary condition

When the boundary condition is not periodic, the proposed scheme needs to be modified for the boundary elements. Without loss of generality, we consider the one dimensional computational domain $(0, a)$ and assume $x_1 = 0$ and $x_N = a$. To impose the boundary condition numerically, at $x = 0$, (2.6) with $i = 1$ will be replaced by

$$\int_{x_1}^{x_{3/2}} \left(\partial_t \varphi_h + H(x, \psi_h, \partial_x\psi_h)\right) \eta dx = \frac{1}{\tau_{\max}} \int_{x_1}^{x_{3/2}} (\psi_h - \varphi_h)\eta dx,$$
$$- H_1(x, \varphi_h, \partial_x\varphi_h)|_{x=x_1} \big(\psi_h(x_1, t) - g_L(t)\big)\eta(x_1)$$

for the inflow boundary condition $\phi(0, t) = g_L(t)$, and by

$$\int_{x_1}^{x_{3/2}} \left(\partial_t \varphi_h + H(x, \psi_h, \partial_x\psi_h)\right) \eta dx = \frac{1}{\tau_{\max}} \int_{x_1}^{x_{3/2}} (\psi_h - \varphi_h)\eta dx$$

for the outflow boundary condition. At $x = a$, (2.6) with $i = N$ will be replaced by

$$\int_{x_{N-\frac{1}{2}}}^{x_N} \left(\partial_t \varphi_h + H(x, \psi_h, \partial_x \psi_h)\right) \eta dx = \frac{1}{\tau_{\max}} \int_{x_{N-\frac{1}{2}}}^{x_N} (\psi_h - \varphi_h)\eta dx, \\ -H_1(x, \varphi_h, \partial_x \varphi_h)|_{x=x_N} \big(g_R(t) - \psi_h(x_N, t)\big)\eta(x_N)$$

for the inflow boundary condition $\phi(a, t) = g_R(t)$, and by

$$\int_{x_{N-\frac{1}{2}}}^{x_N} \left(\partial_t \varphi_h + H(x, \psi_h, \partial_x \psi_h)\right) \eta dx = \frac{1}{\tau_{\max}} \int_{x_{N-\frac{1}{2}}}^{x_N} (\psi_h - \varphi_h)\eta dx$$

for the outflow boundary condition. The boundary condition being inflow or outflow is either given along with the equation, or can be numerically determined as follows: $H_1(x, \varphi_h, \partial_x \varphi_h)|_{x=0} > 0$ (resp. ≤ 0) implies an inflow (resp. outflow) boundary condition at $x = 0$, and $H_1(x, \varphi_h, \partial_x \varphi_h)|_{x=a} < 0$ (resp. ≥ 0) implies an inflow (resp. outflow) boundary condition at $x = a$.

2.2 Nonlinear limiter

It is demonstrated that for some examples with nonconvex Hamiltonians, nonlinear limiters are needed in order for the proposed scheme to capture the viscosity solution. Based on numerical experiments, the following limiting strategy is introduced for P^1 and P^2 approximations: consider three neighboring cells $\{C_1, C_2, C_3\}$, which could be $\{I_i, I_{i+\frac{1}{2}}, I_{i+1}\}$ or $\{I_{i-\frac{1}{2}}, I_i, I_{i+\frac{1}{2}}\}$ for some i. On C_i $(i = 1, 2, 3)$, the numerical solution is represented as $U_i(x) = a_{0,i} + a_{1,i}\xi_i$ for P^1 approximations, and $U_i(x) = a_{0,i} + a_{1,i}\xi_j + a_{2,i}\frac{3\xi_i^2 - 1}{2}$ for P^2 approximations. Here $\xi_i = \frac{x - c_i}{|C_i|/2}$ with c_i being the cell center, and $a_{0,i}$ is the cell average of $U_i(x)$ on C_i. Note the basis functions $1, x, \frac{3x^2-1}{2}$ are the first three Legendre polynomials on $[-1, 1]$. To apply the limiting procedure on C_2,

- we first compute two candidates for the "slope" of $U_2(x)$ in C_2 based on cell averages,

$$s_1 = a_{0,3} - a_{0,2}, \qquad s_2 = a_{0,2} - a_{0,1}.$$

- let $\tilde{a}_{1,2} = \text{minmod}(a_{1,2}, s_1, s_2)$. If $a_{1,2} = \tilde{a}_{1,2}$, no change is needed for $U_2(x)$. Otherwise we replace $U_2(x)$ by

$$\widetilde{U}_2(x) = a_{0,2} + \tilde{a}_{1,2}\xi_2,$$

here

$$\text{minmod}(d_1, d_2, d_3) = \begin{cases} \min\{d_1, d_2, d_3\} & \text{if } d_1, d_2, d_3 > 0, \\ \max\{d_1, d_2, d_3\} & \text{if } d_1, d_2, d_3 < 0, \\ 0 & \text{otherwise.} \end{cases}$$

In the actual implementation, "$a_{1,2} = \tilde{a}_{1,2}$" can be replaced by $|a_{1,2} - \tilde{a}_{1,2}| \leq \epsilon$. For instance in Section 4, $\epsilon = 10^{-7}$ is used for Examples 4.7 and 4.8. This limiting strategy can be regarded as the minmod slope limiter in [13] yet based on two numerical solutions on overlapping meshes. For the P^1 case, it is the same as the nonoscillatory hierarchical reconstruction procedure proposed in [30].

2.3 Time discretization

Up to now we only have the semi-discrete central DG method, resulting the method of lines ODE system

$$\Phi_t = L(\Phi, t), \tag{2.8}$$

where the dependence of $L(\cdot, \cdot)$ on t comes from the numerical boundary condition. This ODE system can be further discretized by total variation diminishing (TVD) Runge-Kutta methods [37, 19]. In Section 4, the following second and third order Runge-Kutta methods are used when $k = 1,\ 2$ in V_h^k (also in W_h^k) respectively. Φ^n (resp. Φ^{n+1}) is the numerical solution of (2.8) at t_n (resp. t_{n+1}), and $\Delta t_n = t_{n+1} - t_n$.

RK2:

$$\begin{aligned} \Phi^{(1)} &= \Phi^n + \Delta t_n L(\Phi^n, t_n), \\ \Phi^{n+1} &= \frac{1}{2}\Phi^n + \frac{1}{2}\Phi^{(1)} + \frac{1}{2}\Delta t_n L(\Phi^{(1)}, t_{n+1}). \end{aligned}$$

RK3:

$$\begin{aligned} \Phi^{(1)} &= \Phi^n + \Delta t_n L(\Phi^n, t_n), \\ \Phi^{(2)} &= \frac{3}{4}\Phi^n + \frac{1}{4}\Phi^{(1)} + \frac{1}{4}\Delta t_n L(\Phi^{(1)}, t_{n+1}), \\ \Phi^{n+1} &= \frac{1}{3}\Phi^n + \frac{2}{3}\Phi^{(2)} + \frac{2}{3}\Delta t_n L(\Phi^{(2)}, t_n + \frac{1}{2}\Delta t_n). \end{aligned}$$

3 Theoretical results

In this section, the L^2 stability and the error estimate will be established for the scheme proposed in Section 2 when the Hamiltonian H in (1.1) is linear. The analysis is closely related to those in [6, 31]. Though only the results for one dimensional cases are presented, similar results can be obtained for multi-dimensional cases.

3.1 L^2 stability

Theorem 3.1. *Consider the one dimensional H-J equation* (1.1) *with* $H(x, \varphi, \partial_x \varphi) = c(x)\partial_x \varphi$ *and with the periodic boundary condition on* $(0, a)$. *Let* $\varphi_h \in V_h$ *and* $\psi_h \in W_h$ *be two numerical solutions of the semi-discrete central DG method* (2.6)-(2.7), *and assume* $\beta = ||c_x||_\infty < \infty$. *Then the following* L^2 *stability holds*

$$E(T) + \int_0^T \frac{1}{\tau_{max}} \Theta(t) e^{-\beta(t-T)} dt \leq E(0) e^{\beta T}, \tag{3.1}$$

where

$$E(t) = \frac{1}{2} \int_0^a \varphi_h^2(x,t) + \psi_h^2(x,t) dx, \qquad \Theta(t) = \int_0^a \left(\varphi_h(x,t) - \psi_h(x,t)\right)^2 dx. \tag{3.2}$$

In particular, when $c(x)$ *is a constant, then*

$$E(T) + \int_0^T \frac{1}{\tau_{max}} \Theta(t) dt = E(0). \tag{3.3}$$

Proof. By taking $H(x, q, p) = c(x)\, p$ in the scheme of (2.6)-(2.7), one gets

$$\int_{I_i} \partial_t \varphi_h \eta dx = -\int_{I_i} c(x) \partial_x \psi_h \eta dx + \frac{1}{\tau_{\max}} \int_{I_i} (\psi_h - \varphi_h) \eta dx - c(x_i)[\psi_h]_i \eta(x_i) \tag{3.4}$$

$$\int_{I_{i+\frac{1}{2}}} \partial_t \psi_h \xi dx = -\int_{I_{i+\frac{1}{2}}} c(x) \partial_x \varphi_h \xi dx + \frac{1}{\tau_{\max}} \int_{I_{i+\frac{1}{2}}} (\varphi_h - \psi_h) \xi dx - c(x_{i+\frac{1}{2}})[\varphi_h]_{i+\frac{1}{2}} \xi(x_{i+\frac{1}{2}}) \tag{3.5}$$

Let $\eta = \varphi_h$ in (3.4) and $\xi = \psi_h$ in (3.5), and sum up (3.4) - (3.5) over i, we get

$$
\begin{aligned}
&\frac{1}{2}\frac{d}{dt}\int_0^a \varphi_h^2+\psi_h^2 dx\\
=&\frac{1}{\tau_{\max}}\int_0^a \left(\psi_h\varphi_h-\varphi_h^2+\varphi_h\psi_h-\psi_h^2\right)dx\\
&-\sum_i\left(\int_{I_i} c(x)\partial_x\psi_h\varphi_h dx+\int_{I_{i+\frac{1}{2}}} c(x)\partial_x\varphi_h\psi_h dx+c(x_i)[\psi_h]_i\varphi_h(x_i)+c(x_{i+\frac{1}{2}})[\varphi_h]_{i+\frac{1}{2}}\psi_h(x_{i+\frac{1}{2}})\right)\\
=&-\frac{1}{\tau_{\max}}\int_0^a(\varphi_h-\psi_h)^2dx+\sum_i\left(\int_{x_{i-\frac{1}{2}}}^{x_i} c_x(x)\psi_h\varphi_h dx+\int_{x_i}^{x_{i+\frac{1}{2}}} c_x(x)\psi_h\varphi_h dx\right)\\
&-\sum_i\left(c(x)\varphi_h\psi_h\Big|_{x_{i-\frac{1}{2}}}^{x_i}+c(x)\psi_h\varphi_h\Big|_{x_i}^{x_{i+\frac{1}{2}}}+c(x_i)[\psi_h]_i\varphi_h(x_i)+c(x_{i+\frac{1}{2}})[\varphi_h]_{i+\frac{1}{2}}\psi_h(x_{i+\frac{1}{2}})\right)\\
=&-\frac{1}{\tau_{\max}}\int_0^a(\varphi_h-\psi_h)^2dx+\int_0^a c_x(x)\varphi_h\psi_h dx\\
&-\sum_i\Big(c(x_i)\varphi_h(x_i)\psi_h(x_i^-)-c(x_{i-\frac{1}{2}})\psi_h(x_{i-\frac{1}{2}})\varphi_h(x_{i-\frac{1}{2}}^+)+c(x_{i+\frac{1}{2}})\psi_h(x_{i+\frac{1}{2}})\varphi_h(x_{i+\frac{1}{2}}^-)\\
&-c(x_i)\varphi_h(x_i)\psi_h(x_i^+)+c(x_i)[\psi_h]_i\varphi_h(x_i)+c(x_{i+\frac{1}{2}})[\varphi_h]_{i+\frac{1}{2}}\psi_h(x_{i+\frac{1}{2}})\Big)\\
=&-\frac{1}{\tau_{\max}}\int_0^a(\varphi_h-\psi_h)^2dx+\int_0^a c_x(x)\varphi_h\psi_h dx
\end{aligned}
$$

Now with $E(t)$ and $\Theta(t)$ defined as (3.2), one gets

$$\frac{d}{dt}E(t)+\frac{1}{\tau_{\max}}\Theta(t)=\int_0^a c_x(x)\varphi_h\psi_h dx. \tag{3.6}$$

If $c(x)$ is a constant, (3.6) becomes

$$\frac{d}{dt}E(t)+\frac{1}{\tau_{\max}}\Theta(t)=0,$$

and integrating in time from 0 to T leads to (3.3).

For more general $c(x)$ with $\beta=||c_x||_\infty<\infty$, (3.6) becomes

$$\frac{d}{dt}E(t)+\frac{1}{\tau_{\max}}\Theta(t)\le\beta E(t),$$

therefore

$$\frac{d}{dt}E(t)-\beta E(t)\le-\frac{1}{\tau_{\max}}\Theta(t). \tag{3.7}$$

Multiplying $e^{-\beta t}$ to both sides of (3.7) and integrating in time from 0 to T, one gets (3.1). □

As pointed out in [31], Theorem 3.1 indicates that the energy dissipation of the proposed scheme is closely related to $\int_0^a \left(\varphi_h(x,t) - \psi_h(x,t)\right)^2 dx$, the L^2 difference of two numerical solutions φ_h and ψ_h. This is different from the standard DG method which evolves one numerical solution, and the energy dissipation is related to the jumps of the numerical solution at element interfaces.

3.2 Error estimate

Theorem 3.2. *Consider the one dimensional H-J equation* (1.1) *with* $H(x, \varphi, \partial_x \varphi) = c\partial_x \varphi$ *and with the periodic boundary condition on* $\Omega = (0, a)$. *Let* φ *denote the exact solution with the initial condition* $\varphi(x, 0) = \varphi_0(x) \in H^{k+1}(\Omega)$, *and* $\varphi_h \in V_h = V_h^k$, $\psi_h \in W_h = W_h^k$ *be two numerical solutions of the semi-discrete central DG method* (2.6)-(2.7). *Then the following* L^2 *error estimate holds*

$$||\varphi - \varphi_h||_{L^2(\Omega)} + ||\varphi - \psi_h||_{L^2(\Omega)} \leq Ch^k. \tag{3.8}$$

Here the constant C *depends on* $||\varphi_0||_{H^{k+1}(\Omega)}$ *and the final time* T.

Based on Remark 2.1, the proposed scheme is exactly the same as the one in [30] when applied to the linear H-J equation with constant coefficient, which is also the linear scalar conservation law equation. And the result (3.8) was established by Theorem 2.2 in [31]. Notice that with respect to the approximation properties of discrete spaces V_h^k and W_h^k, the error estimate (3.8) is suboptimal. In numerical examples however we always observe optimal convergence rates for smooth examples.

4 Numerical examples

In this section we report a sequence of one and two dimensional numerical examples to illustrate the high order accuracy and reliability of the proposed method when approximating the viscosity solutions of H-J equations (1.1). When discretizing (2.6)-(2.7) (or the two dimensional scheme) from time t_n to $t_{n+1} = t_n + \Delta t_n$, $\tau_{\max}$ in the scheme and the time step

Δt_n are computed by

$$\tau_{\max} = dt_n, \qquad \Delta t_n = \theta\, dt_n,$$

with $\theta \in (0, 1]$ as a parameter, and dt_n is dynamically determined by

$$dt_n = \frac{\mathrm{C}_{CFL}\, h_x}{\lambda_{x,n}} \tag{4.1}$$

in one dimensional cases and by

$$dt_n = \mathrm{C}_{CFL} / \left(\frac{\lambda_{x,n}}{h_x} + \frac{\lambda_{y,n}}{h_y} \right) \tag{4.2}$$

in two dimensional cases. Here $\lambda_{x,n} = ||H_1||_\infty$ and $\lambda_{y,n} = ||H_2||_\infty$ at $t = t_n$, and they are computed numerically. $h_x = \min_i(\min(I_i, I_{i+\frac{1}{2}}))$ and $h_y = \min_j(\min(J_j, J_{j+\frac{1}{2}}))$. In the numerical experiments reported below, $\theta = 1$ is taken. Unless specified otherwise, the second order Runge-Kutta method is used for P^1 approximations with $\mathrm{C}_{CFL} = 0.45$, and the third order Runge-Kutta method is used for P^2 approximations with $\mathrm{C}_{CFL} = 0.33$ ([31]).

4.1 One dimensional examples

Example 4.1. We consider the linear advection equation

$$\begin{cases} \varphi_t + \varphi_x = 0, & x \in (0, 2\pi) \\ \varphi(x, 0) = \sin(x) \end{cases}$$

with the smooth initial data and the periodic boundary condition.

For this smooth example, numerical errors and convergence orders are reported in Table 4.1 for P^0, P^1 and P^2 cases. Even though the error estimate in Section 3 shows that the accuracy is suboptimal, we observe optimal $(k+1)$-st order of convergence rate when V_h^k and W_h^k are used. Recall that the proposed scheme is inconsistent when (1.1) is nonlinear (see Remark 2.1), and this is the only example of which numerical results are reported in this paper when $k = 0$.

Example 4.2. We consider the linear advection equation

$$\begin{cases} \varphi_t + \varphi_x = 0, & x \in (-1, 1) \\ \varphi(x, 0) = \varphi_0(x) \end{cases}$$

Table 4.1: Errors and convergence orders for Example 4.1 on a uniform mesh of N cells, $t = 1$

N	L^2 error	Order	L^1 error	Order
		P^0		
10	3.57e-01	-	7.77e-01	-
20	1.72e-01	1.05	3.62e-01	1.10
40	8.35e-02	1.04	1.70e-01	1.09
80	4.13e-02	1.02	8.22e-02	1.05
160	2.05e-02	1.01	4.04e-02	1.02
		P^1		
10	4.33e-02	-	8.72e-02	-
20	1.05e-02	2.05	2.12e-02	2.04
40	2.55e-03	2.04	5.18e-03	2.04
80	6.09e-04	2.06	1.24e-03	2.06
160	1.63e-04	1.91	3.29e-04	1.92
		P^2		
10	1.68e-03	-	3.33e-03	-
20	2.17e-04	2.96	4.03e-04	3.05
40	2.58e-05	3.07	4.81e-05	3.07
80	3.40e-06	2.92	6.10e-06	2.98
160	4.17e-07	3.03	7.49e-07	3.02

with the periodic boundary condition and the nonsmooth initial data

$$\varphi_0(x) = -\left(\frac{\sqrt{3}}{2} + \frac{9}{2} + \frac{2\pi}{3}\right)(x+1) + \begin{cases} 2\cos(\frac{3\pi x^2}{2}) - \sqrt{3}, & -1 \le x < -\frac{1}{3} \\ \frac{3}{2} + 3\cos(2\pi x), & -\frac{1}{3} \le x < 0 \\ \frac{15}{2} - 3\cos(2\pi x), & 0 \le x < \frac{1}{3} \\ \frac{28+4\pi+\cos(3\pi x)}{3} + 6\pi x(x-1), & \frac{1}{3} \le x < 1 \end{cases}$$

This example is used to illustrate the dissipative properties of the proposed method. Figure 4.1 (resp. Figure 4.2) includes the exact solution as well as the P^1 (resp. P^2) numerical solutions after one time period (left) and after four time periods (right), and the features of the solution are well captured by the method. In addition, one can see that the scheme has smaller numerical dissipation when using higher degrees of polynomials as approximations. Generally this is common when lower order methods are compared with

higher order methods.

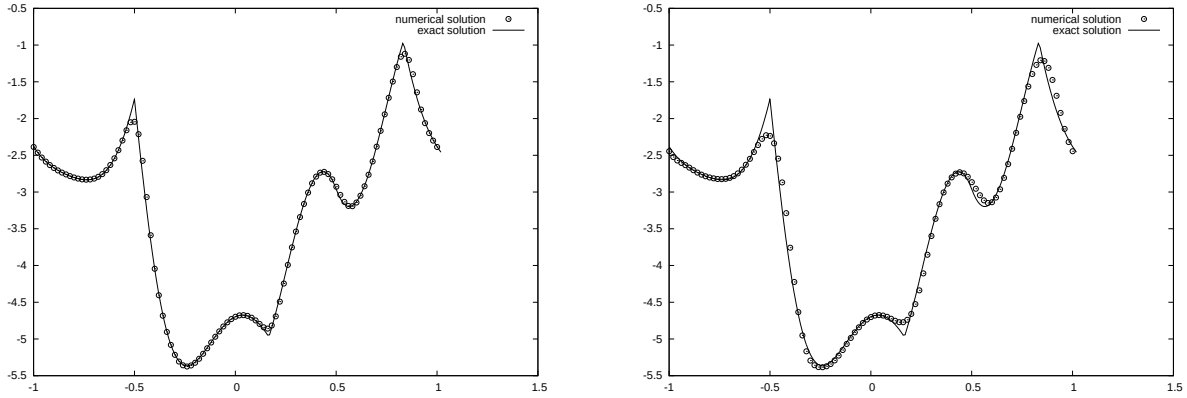

Figure 4.1: Example 4.2. $t = 2$ (left), $t = 8$ (right), $N = 100$, using P^1 polynomials.

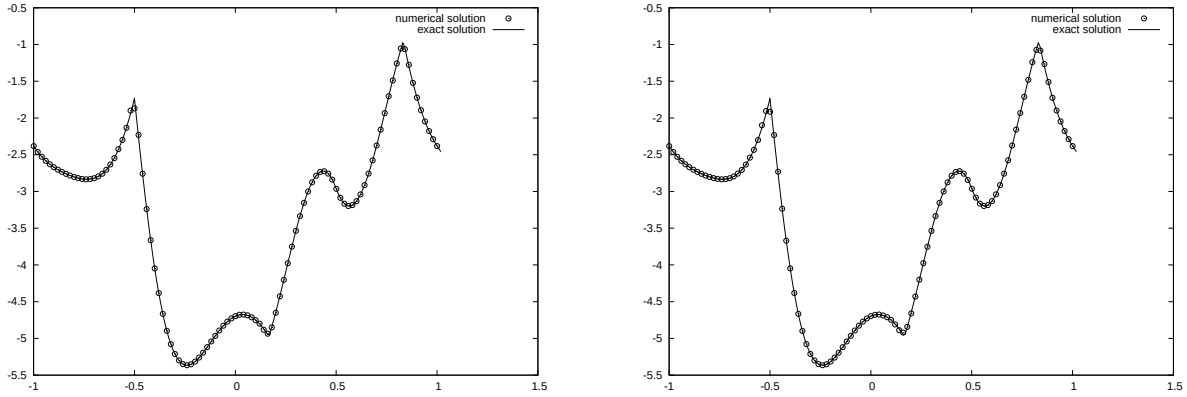

Figure 4.2: Example 4.2. $t = 2$ (left), $t = 8$ (right), $N = 100$, using P^2 polynomials.

Example 4.3. We consider the following linear equation

$$\begin{cases} \varphi_t + \text{sign}(\cos(x))\varphi_x = 0, \quad x \in (0, 2\pi) \\ \varphi(x, 0) = \sin(x) \end{cases}$$

with the nonsmooth coefficient and the periodic boundary condition. The exact solution is piecewise smooth and its formula can be found in [6].

The numerical solution at $t = 1$ is plotted in Figure 4.3, and it approximates well the exact solution, which contains a shock in φ_x at $x = \frac{\pi}{2}$ and a rarefaction wave around $x = \frac{3\pi}{2}$. Errors and convergence orders in Table 4.2 are computed in $(0, 2\pi)\backslash[1.5, 1.64]$ where the exact solution is H^2. The order of accuracy in this subregion is expected to be $\min(2, k+1)$.

We want to mention that the direct DG method introduced in [6] needs an entropy correction procedure in order to capture the viscosity solution for this example.

Table 4.2: Errors and convergence orders for Example 4.3 on a uniform mesh of N cells, computed in the subregion $(0, 2\pi)\backslash[1.5, 1.64]$, $t = 1$

N	L^2 error	Order	L^1 error	Order
		P^1		
10	1.02e-01	-	1.82e-01	-
20	3.80e-02	1.42	6.59e-02	1.47
40	1.18e-02	1.69	1.95e-02	1.76
80	3.42e-03	1.78	5.22e-03	1.90
160	7.47e-04	2.19	1.25e-03	2.06
		P^2		
10	3.77e-02	-	5.82e-02	-
20	9.62e-03	1.97	1.35e-02	2.10
40	2.44e-03	1.98	3.41e-03	1.99
80	9.34e-04	1.38	9.52e-04	1.84
160	1.40e-04	2.74	2.01e-04	2.25

Example 4.4. We consider the Burgers' equation

$$\begin{cases} \varphi_t + \frac{1}{2}(\varphi_x)^2 = 0, & x \in (0, 2\pi) \\ \varphi(x, 0) = -\cos(x) \end{cases}$$

with the periodic boundary condition and the smooth initial data. The Hamiltonian is nonlinear and convex.

At $t = 0.5$, the exact solution is smooth, and the optimal order of accuracy of the proposed scheme is observed for both P^1 and P^2 approximations in Table 4.3. Later a shock is formed in φ_x, and it is approximated sharply by the scheme, see Figure 4.4 for the solution at $t = 1$. In Table 4.4, errors and convergence orders at $t = 1$ are reported, and they are computed in $(0, 2\pi)\backslash[3.0, 3.28]$. The solution in this region is smooth and the numerical results again show optimal accuracy.

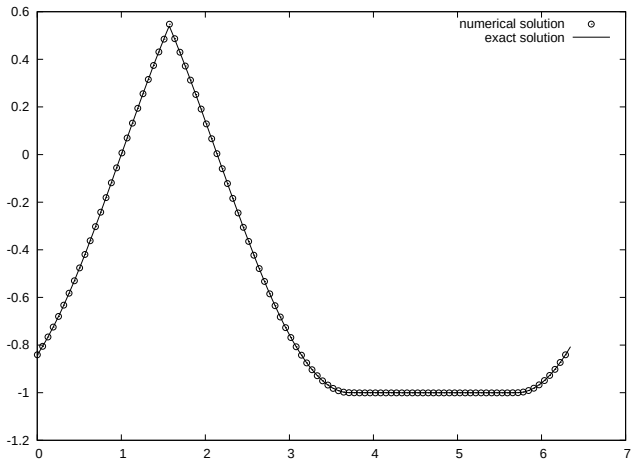

Figure 4.3: Example 4.3. $t = 1$, $N = 100$, using P^2 polynomials.

Table 4.3: Errors and convergence orders for Example 4.4 on a uniform mesh of N cells, $t = 0.5$

N	L^2 error	Order	L^1 error	Order
		P^1		
10	2.87e-02	-	4.97e-02	-
20	7.67e-03	1.91	1.35e-02	1.88
40	2.04e-03	1.91	3.61e-03	1.90
80	4.84e-04	2.08	8.56e-04	2.08
160	1.16e-04	2.06	2.05e-04	2.06
		P^2		
10	2.26e-03	-	3.09e-03	-
20	3.00e-04	2.91	4.07e-04	2.93
40	4.12e-05	2.86	5.56e-05	2.87
80	5.04e-06	3.03	6.72e-06	3.05
160	6.53e-07	2.95	8.51e-07	2.98

Example 4.5. We consider the Eikonal equation

$$\begin{cases} \varphi_t + |\varphi_x| = 0, & x \in (0, 2\pi) \\ \varphi(x, 0) = \sin(x) \end{cases}$$

with the periodic boundary condition and the smooth initial data. The Hamiltonian is nonsmooth and convex. This example has the same exact solution as Example 4.3. Numerical errors and convergence orders are reported in Table 4.5, which are computed in

Table 4.4: Errors and convergence orders for Example 4.4 on a uniform mesh of N cells, computed in the subregion $(0, 2\pi)\backslash[3.0, 3.28]$, $t = 1$

N	L^2 error	Order	L^1 error	Order
		P^1		
10	2.88e-02	-	5.18e-02	-
20	8.67e-03	1.73	1.37e-02	1.92
40	2.71e-03	1.68	3.70e-03	1.89
80	4.14e-04	2.71	7.64e-04	2.28
160	1.03e-04	2.00	1.91e-04	2.00
		P^2		
10	3.57e-03	-	3.03e-03	-
20	1.06e-03	1.75	7.01e-04	2.11
40	3.53e-04	1.59	1.84e-04	1.93
80	1.79e-05	4.31	8.57e-06	4.43
160	8.00e-07	4.48	6.08e-07	3.82

$(0, 2\pi)\backslash[1.5, 1.64]$ where the exact solution is H^2. The order of accuracy in this subregion is expected to be $\min(2, k + 1)$. Unlike in [6], the entropy correction procedure is not needed for the proposed method to capture the viscosity solution.

Table 4.5: Errors and convergence orders for Example 4.5 on a uniform mesh of N cells, computed in the subregion $(0, 2\pi)\backslash[1.5, 1.64]$, $t = 1$

N	L^2 error	Order	L^1 error	Order
		P^1		
10	1.14e-01	-	2.13e-01	-
20	2.51e-02	2.18	4.14e-02	2.36
40	8.76e-03	1.52	1.34e-02	1.63
80	2.77e-03	1.66	3.82e-03	1.81
160	6.57e-04	2.07	1.03e-03	1.89
		P^2		
10	3.78e-02	-	6.44e-02	-
20	1.09e-02	1.79	1.65e-02	1.97
40	3.19e-03	1.77	4.70e-03	1.81
80	1.17e-03	1.44	1.46e-03	1.69
160	2.68e-04	2.13	3.87e-04	1.92

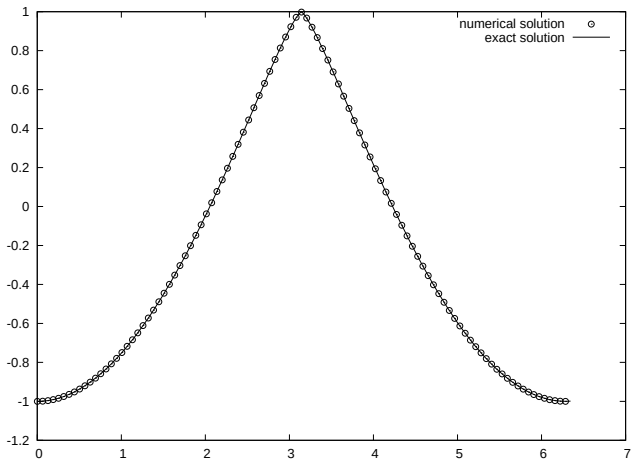

Figure 4.4: Example 4.4. $t = 1$, $N = 100$, using P^2 polynomials.

Example 4.6. The following example

$$\begin{cases} \varphi_t - \cos(\varphi_x + 1) = 0, \quad x \in (-1, 1) \\ \varphi(x, 0) = -\cos(\pi x) \end{cases}$$

involves a nonconvex Hamiltonian with the smooth initial data. The boundary condition is periodic.

At $t = 0.5/\pi^2$, the exact solution is smooth, and numerical results are presented in Table 4.6, demonstrating the optimal order of accuracy of the proposed method. By the time $t = 1.5/\pi^2$, nonsmooth features have developed in φ, and they are reliably captured, see Figure 4.5.

Example 4.7. We consider the Riemann problem with a nonconvex Hamiltonian

$$\begin{cases} \varphi_t + \frac{1}{4}(\varphi_x^2 - 1)(\varphi_x^2 - 4) = 0, \quad x \in (-1, 1) \\ \varphi(x, 0) = -2|x|. \end{cases}$$

Similarly as observed in [20], a nonlinear limiter is needed in order for the proposed scheme to capture the viscosity solution of this example. This can be seen from Figure 4.6, which contains the exact solution as well as the numerical solutions with (left) and without (right) the limiting step. The limiter procedure used here is described in Section 2.2. Due

Table 4.6: Errors and convergence orders for Example 4.6 on a uniform mesh of N cells, $t = 0.5/\pi^2$

N	L^2 error	Order	L^1 error	Order
		P^1		
10	2.10e-02	-	2.17e-02	-
20	4.63e-03	2.18	4.80e-03	2.17
40	1.14e-03	2.02	1.15e-03	2.06
80	2.76e-04	2.05	2.77e-04	2.05
160	6.91e-05	2.00	6.93e-05	2.00
		P^2		
10	1.38e-03	-	1.55e-03	-
20	2.40e-04	2.53	2.22e-04	2.81
40	2.71e-05	3.14	2.35e-05	3.24
80	3.36e-06	3.01	2.86e-06	3.04
160	4.15e-07	3.02	3.45e-07	3.05

to the low regularity of the exact solution, both P^1 and P^2 approximations are of first order accuracy, see Table 4.7. For P^2 case, $C_{CFL} = 0.2$ is taken to determine the time step by (4.1). Note the P^2 results have larger errors, and this can be explained by the nonlinear limiter adopted in the computation. In fact, when this limiter is used in some element I_i, the P^2 numerical solution in I_i will be replaced with a linear polynomial. On the other hand, it is observed that in the P^2 simulation, the limiter was applied in the central region where the exact solution is not linear. This implies that P^1 and P^2 approximations will have comparable *spatial* errors for this example, and this is confirmed by the results in Table 4.8 when the same time discretization, the third order Runge-Kutta method with the fixed time-step $\Delta t = C_{CFL} h_x/\lambda_x$ as well as $C_{CFL} = 0.18$ and $\lambda_x = 3.5$ (an upper bound for $||H_1||_\infty$ in the (x, t) domain), is applied in P^1 and P^2 simulations. The computation is carried out with the outflow numerical boundary condition (see Section 2.1). Other nonlinear limiters that were tested yet failed to capture the viscosity solution for *both* P^1 and P^2 computations include the minmod slope limiter in [13] and the nonoscillatory hierarchical reconstruction procedure in [30]. Further investigation is needed to identify other robust limiting strategies for the

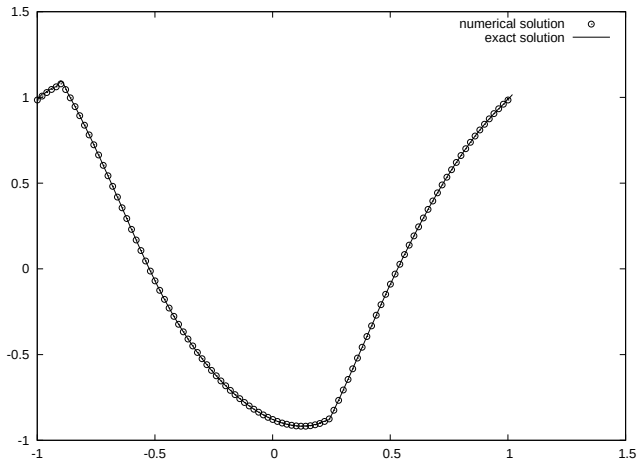

Figure 4.5: Example 4.6. $t = 1.5/\pi^2$, $N = 100$, using P^2 polynomials.

proposed scheme when Hamiltonians are nonconvex and when higher order polynomials are used.

Table 4.7: Errors and convergence orders for Example 4.7 on a uniform mesh of N cells, $t = 1$. The second order Runge-Kutta method is used for P^1 approximations with $C_{CFL} = 0.45$, and the third order Runge-Kutta method is used for P^2 approximations with $C_{CFL} = 0.2$. The time step $\Delta t_n = \theta dt_n$ is dynamically determined by (4.1) with $\theta = 1$.

N	L^2 error	Order	L^1 error	Order
		P^1		
10	2.06e-01	-	2.61e-01	-
20	1.05e-01	0.97	1.14e-01	1.19
40	5.31e-02	0.98	5.67e-02	1.01
80	2.66e-02	0.99	2.78e-02	1.03
160	1.33e-02	1.00	1.38e-02	1.01
		P^2		
10	4.18e-01	-	5.33e-01	-
20	2.24e-01	0.90	2.57e-01	1.05
40	1.14e-01	0.98	1.24e-01	1.06
80	5.72e-02	0.99	6.06e-02	1.03
160	2.85e-02	1.00	2.98e-02	1.02

Table 4.8: Errors and convergence orders for Example 4.7 on a uniform mesh of N cells, $t = 1$. The third order Runge-Kutta method is used for *both* P^1 and P^2 approximations, with the fixed time step $\Delta t = C_{CFL} h_x/\lambda_x$, and $C_{CFL} = 0.18$, $\lambda_x = 3.5$, $h_x = \min_i(\min(I_i, I_{i+\frac{1}{2}}))$.

N	L^2 error	Order	L^1 error	Order
		P^1		
10	3.74e-01	-	4.98e-01	-
20	1.84e-01	1.03	2.06e-01	1.27
40	9.31e-02	0.98	1.00e-01	1.04
80	4.67e-02	1.00	4.92e-02	1.03
160	2.33e-02	1.00	2.43e-02	1.02
		P^2		
10	3.77e-01	-	4.90e-01	-
20	1.87e-01	1.01	2.12e-01	1.21
40	9.48e-02	0.98	1.02e-01	1.05
80	4.75e-02	1.00	5.01e-02	1.03
160	2.37e-02	1.00	2.47e-02	1.02

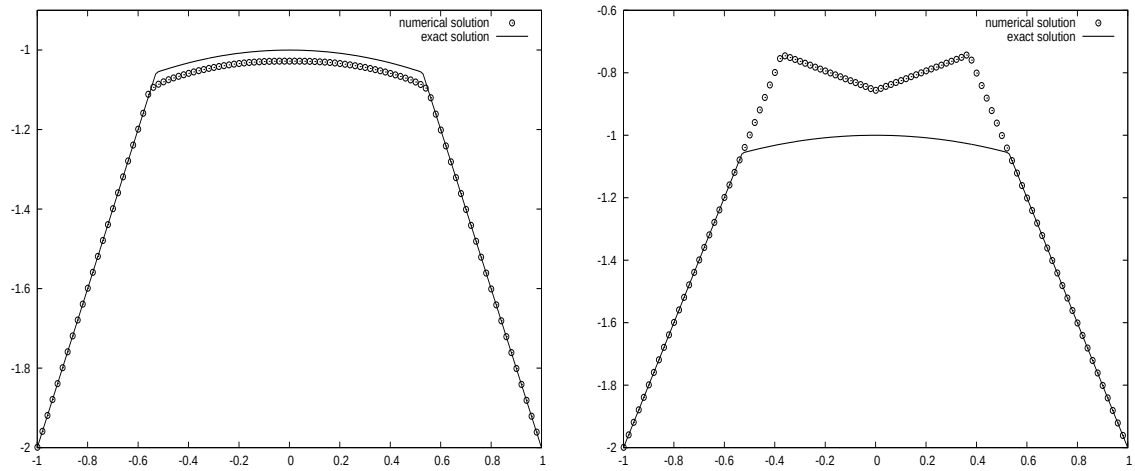

Figure 4.6: Example 4.7. $t = 1$, $N = 100$, using P^2 polynomials with (left) and without limiting (right).

Example 4.8. We consider another nonconvex example

$$\begin{cases} \varphi_t + H(\varphi_x) = 0, & x \in (0,1) \\ \varphi(x,0) = \varphi_0(x), \end{cases}$$

with the Hamiltonian

$$H(u) = \begin{cases} \frac{1}{4}u(1-u), & u \le \frac{1}{2} \\ \frac{1}{2}u(u-1) + \frac{3}{16}, & u > \frac{1}{2} \end{cases}$$

and the initial condition

$$\varphi_0(x) = \begin{cases} x - \frac{1}{4}, & x \leq \frac{1}{4} \\ 0, & x > \frac{1}{4}. \end{cases}$$

The exact viscosity solution is composed (from left to right) of a linear part, a parabolic part and a constant state, and the nonlinear limiter turns out to be necessary for capturing this solution. This can be seen from Figure 4.7, which contains the exact solution and the numerical solution with the limiting step (left), and the zoomed-in plots of the exact solution and numerical solutions with and without the limiting step (right). The limiter procedure used here is described in Section 2.2. In the computation, the outflow numerical boundary condition is applied. Similar to Example 4.7, it is observed that the nonlinear limiter is used in the parabolic section of the solution in all simulations, and therefore we here only report the results (see Table 4.9) when both P^1 and P^2 computations are performed with the same time discretization, that is, the third order Runge-Kutta method with the fixed time-step $\Delta t = C_{CFL} h_x/\lambda_x$ as well as $C_{CFL} = 0.18$ and $\lambda_x = 0.5$ (an estimate for $||H_1||_\infty$ in the (x,t) domain). Note both P^1 and P^2 approximations are comparable and they are of first order accuracy due to the low regularity of the exact solution. This example was also discussed in [4] to illustrate the role of nonlinear limiters in capturing viscosity solutions.

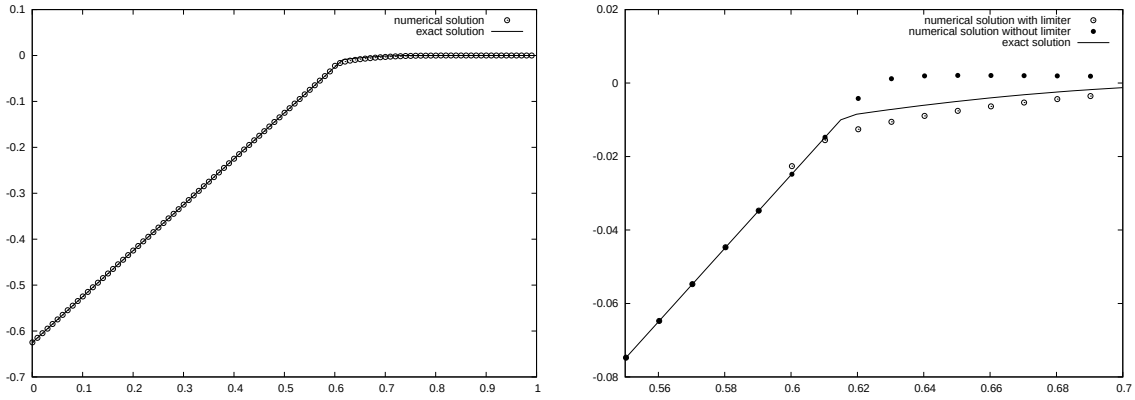

Figure 4.7: Example 4.8. $t = 2$, $N = 100$, using P^2 polynomials. The solution with limiting (left), zoomed in comparison of solutions with and without limiting (right).

Table 4.9: Errors and convergence orders for Example 4.8 on a uniform mesh of N cells, $t = 2$. The third order Runge-Kutta method is used for *both* P^1 and P^2 approximations, with the fixed time step $\Delta t = C_{CFL} h_x/\lambda_x$, and $C_{CFL} = 0.18$, $\lambda_x = 0.5$, $h_x = \min_i(\min(I_i, I_{i+\frac{1}{2}}))$.

N	L^2 error	Order	L^1 error	Order
		P^1		
10	2.15e-02	-	1.94e-02	-
20	5.73e-03	1.91	2.93e-03	2.72
40	2.84e-03	1.01	1.23e-03	1.25
80	1.40e-03	1.02	5.43e-04	1.18
160	6.87e-04	1.03	2.45e-04	1.15
		P^2		
10	1.57e-02	-	1.41e-02	-
20	5.72e-03	1.46	3.32e-03	2.09
40	2.81e-03	1.02	1.22e-03	1.45
80	1.39e-03	1.02	5.35e-04	1.18
160	6.79e-04	1.03	2.42e-04	1.14

4.2 Two dimensional examples

Example 4.9. We consider the linear advection equation

$$\begin{cases} \varphi_t + \varphi_x + \varphi_y = 0, & (x, y) \in (-1, 1)^2 \\ \varphi(x, y, 0) = \sin(\pi(x + y)) \end{cases}$$

with the periodic boundary condition and the smooth initial data.

This can be regarded as a rotated one dimensional advection equation in two dimensional space. Similarly as in one dimensional case, the numerical results reported in Table 4.10 show the optimal convergence property of the proposed method for this smooth example.

Example 4.10. We consider the Burgers' equation

$$\begin{cases} \varphi_t + \frac{1}{2}(\varphi_x + \varphi_y)^2 = 0, & (x, y) \in (0, 2\pi)^2 \\ \varphi(x, y, 0) = -\cos(x + y) \end{cases}$$

with the smooth initial data.

We first assume the boundary condition is periodic. At $t = 0.1$, the exact solution is still smooth, and the proposed scheme demonstrates the optimal convergent behavior in

Table 4.10: Errors and convergence orders for Example 4.9 on a uniform mesh of $N \times N$ cells, $t = 1$

N	L^2 error	Order	L^1 error	Order
		P^1		
10	5.23e-02	-	4.64e-02	-
20	1.55e-02	1.76	1.38e-02	1.75
40	4.05e-03	1.93	3.61e-03	1.93
80	1.02e-03	1.99	9.10e-04	1.99
160	2.56e-04	2.00	2.28e-04	2.00
		P^2		
10	3.41e-03	-	2.86e-03	-
20	4.28e-04	2.99	3.52e-04	3.02
40	5.14e-05	3.06	4.26e-05	3.05
80	6.53e-06	2.98	5.38e-06	2.98
160	8.52e-07	2.94	6.95e-07	2.95

Table 4.11. Later at $t = 0.5$, nonsmooth features form in the solution which are reliably approximated, see Figure 4.8. For the same exact solution, the computation is also carried out with the non-periodic boundary condition based on Section 2.1. The results at $t = 0.1$ are reported in Table 4.12, and they further confirm the optimal convergence property of the method.

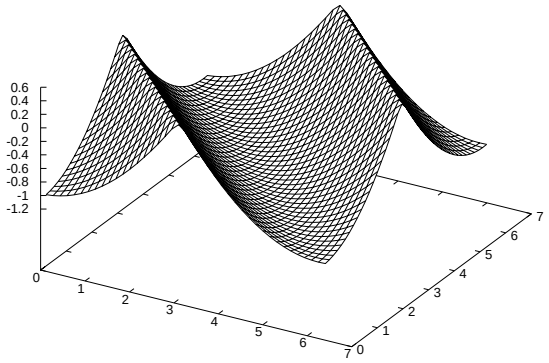

Figure 4.8: Example 4.10. $t = 0.5$, $N \times N = 40 \times 40$, using P^2 polynomials.

Table 4.11: Errors and convergence orders for Example 4.10 on a uniform mesh of $N \times N$ cells, $t = 0.1$, periodic boundary condition

N	L^2 error	Order	L^1 error	Order
		P^1		
10	2.23e-02	-	1.32e-02	-
20	6.79e-03	1.72	4.19e-03	1.65
40	1.56e-03	2.12	9.40e-04	2.16
80	3.67e-04	2.08	2.19e-04	2.10
160	9.09e-05	2.01	5.40e-05	2.02
		P^2		
10	3.45e-03	-	2.11e-03	-
20	4.76e-04	2.86	3.01e-04	2.81
40	5.74e-05	3.05	3.44e-05	3.13
80	6.81e-06	3.07	3.91e-06	3.14
160	8.83e-07	2.95	5.08e-07	2.94

Table 4.12: Errors and convergence orders for Example 4.10 on a uniform mesh of $N \times N$ cells, $t = 0.1$, non-periodic boundary condition

N	L^2 error	Order	L^1 error	Order
		P^1		
10	2.24e-02	-	1.34e-02	-
20	6.82e-03	1.72	4.21e-03	1.67
40	1.57e-03	2.12	9.46e-04	2.15
80	3.70e-04	2.08	2.20e-04	2.11
160	9.16e-05	2.01	5.42e-05	2.02
		P^2		
10	3.46e-03	-	2.09e-03	-
20	4.79e-04	2.85	3.03e-04	2.79
40	5.80e-05	3.04	3.49e-05	3.12
80	6.96e-06	3.06	4.03e-06	3.12
160	9.21e-07	2.92	5.32e-07	2.92

Example 4.11. We consider the following nonlinear example

$$\begin{cases} \varphi_t + \varphi_x \varphi_y = 0, & (x, y) \in (-\pi, \pi)^2 \\ \varphi(x, y, 0) = \sin(x) + \cos(y) \end{cases}$$

with the periodic boundary condition. Different from Examples 4.9 and 4.10, this example is

genuinely two dimensional. Figure 4.9 shows how the numerical solutions look like when the exact solution is smooth (left, at $t = 0.8$), and when singular features form in the solution (right, at $t = 1.5$). Errors and convergence orders are presented in Table 4.13 at $t = 0.8$, demonstrating the optimal convergence property of the proposed method.

Table 4.13: Errors and convergence orders for Example 4.11 on a uniform mesh of $N \times N$ cells, $t = 0.8$

N	L^2 error	Order	L^1 error	Order
		P^1		
10	2.61e-02	-	1.87e-02	-
20	6.86e-03	1.93	4.74e-03	1.98
40	1.72e-03	2.00	1.18e-03	2.00
80	4.22e-04	2.02	2.92e-04	2.02
160	1.05e-04	2.01	7.30e-05	2.00
		P^2		
10	3.92e-03	-	2.13e-03	-
20	4.46e-04	3.14	2.40e-04	3.15
40	6.30e-05	2.82	3.15e-05	2.93
80	7.99e-06	2.98	3.90e-06	3.01
160	9.96e-07	3.00	4.77e-07	3.03

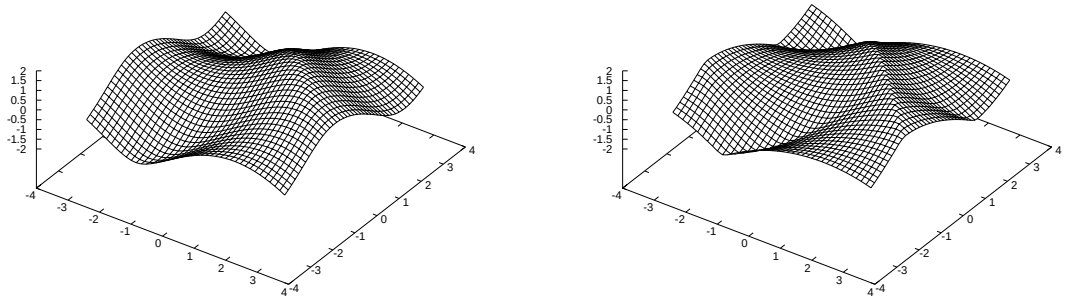

Figure 4.9: Example 4.11. $t = 0.8$ (left), $t = 1.5$ (right), $N \times N = 40 \times 40$, using P^2 polynomials.

Example 4.12. This example is related to controlling optimal cost determination, see [34]

$$\begin{cases} \varphi_t + \sin(y)\varphi_x + (\sin(x) + \text{sign}(\varphi_y))\,\varphi_y - \frac{1}{2}\sin^2(y) + \cos(x) - 1 = 0, \quad (x,y) \in (-\pi,\pi)^2 \\ \varphi(x,y,0) = 0. \end{cases}$$

The boundary condition is periodic and the Hamiltonian is nonsmooth. The numerical solution (left) and the optimal control $\omega = \text{sign}(\varphi_y)$ (right) at $t = 1$ are shown in Figure 4.10. The results are comparable to those by the DG methods in [20] and the WENO methods in [40].

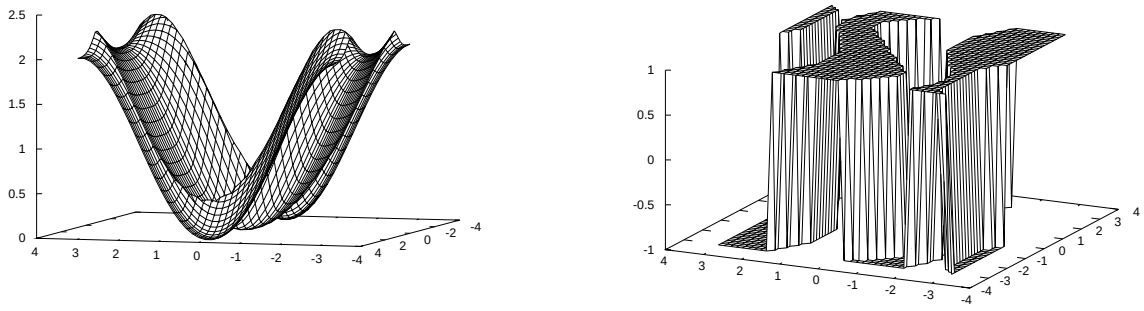

Figure 4.10: Example 4.12. The numerical solution (left) and the optimal control $\text{sign}(\varphi_y)$ (right). $t = 1$, $N \times N = 40 \times 40$, using P^2 polynomials.

5 Concluding remarks

A central discontinuous Galerkin method is proposed in this paper to solve Hamilton-Jacobi equations. The method is motivated by the "weighted-residual" or "stabilization-based" formulation of central discontinuous Galerkin methods when applied to hyperbolic conservation laws [28, 30, 31]. The L^2 stability and the error estimate are established for linear Hamiltonians. And the high order accuracy and reliability of the proposed method, when approximating the viscosity solutions of more general Hamilton-Jacobi equations, are demonstrated through a series of numerical experiments. More investigation is needed to identify other robust nonlinear limiting strategies particularly suitable for the proposed method to

capture the viscosity solutions when Hamiltonians are nonconvex and when higher order polynomials are used. The suboptimal error estimate for linear cases can also be further improved.

References

[1] D.N. Arnold, F. Brezzi, B. Cockburn and L.D. Marini, *Unified analysis of discontinuous Galerkin methods for elliptic problems*, SIAM Journal on Numerical Analysis, v39 (2001/02), pp.1749–1779.

[2] B. Ayuso and L.D. Marini, *Discontinuous Galerkin Methods for Advection-diffusion-reaction problems*, SIAM Journal on Numerical Analysis, v47 (2009), pp.1391–1420.

[3] F. Brezzi, B. Cockburn, L.D. Marini and E. Süli, *Stabilization mechanisms in discontinuous Galerkin finite element methods*, Computer Methods in Applied Mechanics and Engineering, v195 (2006), pp.3293–3310.

[4] S. Bryson and D. Levy, *Mapped WENO and weighted power ENO reconstruction in semi-discrete central schemes for Hamilton-Jacobi equations*, Applied Numerical Mathematics, v56 (2006), pp.1211–1224.

[5] S. Bryson and D. Levy, *High-order semi-discrete central-upwind schemes for multidimensional Hamilton-Jacobi equations*, Journal of Computational Physics, v189 (2003), pp.63-87.

[6] Y. Cheng and C.-W. Shu, *A discontinuous Galerkin finite element method for directly solving the Hamilton-Jacobi equations*, Journal of Computational Physics, v223 (2007), pp.398-415.

[7] B. Cockburn, S. Hou and C.-W. Shu, *The Runge-Kutta local projection discontinuous Galerkin finite element method for conservation laws IV: the multidimensional case*, Mathematics of Computation, 54 (1990), 545–581.

[8] B. Cockburn, G. Karniadakis and C.-W. Shu, *The development of discontinuous Galerkin methods*, in *Discontinuous Galerkin Methods: Theory, Computation and Applications*, B. Cockburn, G. Karniadakis and C.-W. Shu, editors, Lecture Notes in Computational Science and Engineering, volume 11, Springer, 2000.

[9] B. Cockburn, F. Li and C.-W. Shu, *Locally divergence-free discontinuous Galerkin methods for the Maxwell equations*, Journal of Computational Physics, v194 (2004), pp.588-610.

[10] B. Cockburn, S.-Y. Lin and C.-W. Shu, *TVB Runge-Kutta local projection discontinuous Galerkin finite element method for conservation laws III: One-dimensional systems*, Journal of Computational Physics, v84 (1989), 90–113.

[11] B. Cockburn and C.-W. Shu, *TVB Runge-Kutta local projection discontinuous Galerkin finite element method for conservation laws II: general framework*, Mathematics of Computation, v52 (1989), pp.411-435.

[12] B. Cockburn and C.-W. Shu, *The Runge-Kutta local projection P1-discontinuous Galerkin finite element method for scalar conservation laws*, Mathematical Modelling and Numerical Analysis, v25 (1991), 337–361.

[13] B. Cockburn and C.-W. Shu, *The Runge-Kutta discontinuous Galerkin method for conservation laws V: multidimensional systems*, Journal of Computational Physics, v141 (1998), 199–224.

[14] B. Cockburn and C.-W. Shu, special issue on discontinuous Galerkin methods, Journal of Scientific Computing, v22-23 (2005).

[15] M.G. Crandall, L.C. Evans and P.L. Lions, *Some properties of viscosity solutions of Hamilton-Jacobi equations*, Transactions of the American Mathematical Society, v282 (1984), pp. 487–502.

[16] M. Crandall and P.L. Lions, *Viscosity solutions of Hamilton-Jacobi equations*, Transactions of the American Mathematical Society, v277 (1983), pp.1-42.

[17] M. Crandall and P.L. Lions, *Two Approximations of solutions of Hamilton-Jacobi equations*, Mathematics of Computation, v43 (1984), pp.1-19.

[18] L.C. Evans, *Partial differential equations*, American Mathematical Society, 1998.

[19] S. Gottlieb, C.-W. Shu and E. Tadmor, *Strong stability-preserving high-order time discretization methods*, SIAM Review, v43 (2001), pp.89–112.

[20] C. Hu and C.-W. Shu, *A discontinuous Galerkin finite element method for Hamilton-Jacobi equations*, SIAM Journal on Scientific Computing, v21 (1999), pp.666-690.

[21] G.-S. Jiang and D. Peng, *Weighted ENO schemes for Hamilton-Jacobi equations*, SIAM Journal on Scientific Computing, v21 (2000), pp.2126-2143.

[22] A. Kurganov, S. Noelle and G. Petrova, *Semidiscrete central-upwind schemes for hyperbolic conservation laws and Hamilton-Jacobi equations*, SIAM Journal on Scientific Computing, v23 (2001), pp. 707–740.

[23] A. Kurganov and E. Tadmor, *New high-resolution central schemes for nonlinear conservation laws and convection-diffusion equations*, Journal of Computational Physics, v160 (2000), pp.214–282.

[24] A. Kurganov and E. Tadmor, *New high-resolution semi-discrete central schemes for Hamilton-Jacobi equations*, Journal of Computational Physics, v160 (2000), pp. 720-742.

[25] O. Lepsky, C. Hu and C.-W. Shu, *Analysis of the discontinuous Galerkin method for Hamilton-Jacobi equations*, Applied Numerical Mathematics, v33 (2000), pp.423-434.

[26] R.J. Leveque, *Finite volume methods for hyperbolic problems*, Cambridge University Press, 2002.

[27] F. Li and C.-W. Shu, *Reinterpretation and simplified implementation of a discontinuous Galerkin method for Hamilton-Jacobi equations*, Applied Mathematics Letters, v18 (2005), pp.1204-1209.

[28] Y.-J. Liu, *Central schemes and central discontinuous Galerkin methods on overlapping cells*, Conference on Analysis, Modeling and Computation of PDE and Multiphase Flow, Stony Brook, NY, 2004.

[29] Y.-J. Liu, *Central schemes on overlapping cells*, Journal of Computational Physics, v209 (2005), pp.82–104.

[30] Y.-J. Liu, C.-W. Shu, E. Tadmor and M. Zhang, *Central discontinuous Galerkin methods on overlapping cells with a nonoscillatory hierarchical reconstruction*, SIAM Journal on Numerical Analysis, v45 (2007), pp.2442–2467.

[31] Y.-J. Liu, C.-W. Shu, E. Tadmor and M. Zhang, *L^2 stability analysis of the central discontinuous Galerkin method and a comparison between the central and regular discontinuous Galerkin methods*, ESAIM: Mathematical Modelling and Numerical Analysis, v42 (2008), pp.593-607.

[32] H. Nessyahu and E. Tadmor, *Non-oscillatory central differencing for hyperbolic conservation laws*, Journal of Computational Physics, v87 (1990), pp.408–463.

[33] S. Osher and J. Sethian, *Fronts propagating with curvature dependent speed: algorithms based on Hamilton-Jacobi formulations*, Journal of Computational Physics, v79 (1988), pp.12-49.

[34] S. Osher and C.-W. Shu, *High-order essentially nonoscillatory schemes for Hamilton-Jacobi equations*, SIAM Journal on Numerical Analysis, v28 (1991), pp.907-922.

[35] J. Qiu and C.-W. Shu, *Hermite WENO schemes for Hamilton-Jacobi equations*, Journal of Computational Physics, v204 (2005), pp. 82-99.

[36] W.H. Reed and T.R. Hill, *Triangular mesh methods for the neutron transport equation*, Technical Report LA-UR-73-479, Los Alamos Scientific Laboratory, 1973.

[37] C.-W. Shu, *Total-Variation-Diminishing time discretizations*, SIAM Journal on Scientific and Statistical Computing, v9 (1988), pp.1073-1084.

[38] P.E. Souganidis, *Approximation schemes for viscosity solutions of Hamilton-Jacobi equations*, Journal of Differential Equations, v59 (1985), pp.1–43.

[39] L. Yuan and C.-W. Shu, *Discontinuous Galerkin method based on non-polynomial approximation spaces*, Journal of Computational Physics, v218 (2006), pp.295–323.

[40] Y.-T. Zhang and C.-W. Shu, *High-order WENO schemes for Hamilton-Jacobi equations on triangular meshes*, SIAM Journal on Scientific Computing, v24 (2003), pp.1005-1030.